Nonlinear Dynamics **24:** 129–146, 2001.

Analytical and Experimental Analysis of Wing Rock

G. GUGLIERI and F. B. QUAGLIOTTI
Dipartimento di Ingegneria Aeronautica e Spaziale, Politecnico di Torino, 10129 Torino, Italy

(Received: 9 September 1998; accepted: 30 May 2000)

Abstract. The paper deals with the study of an analytical model of wing rock, based on parameter identification of experimental data. The experiments were performed in the Aeronautical Laboratory of Politecnico di Torino, in the D3M Low Speed Wind Tunnel, on a 80° delta wing. Free-to-roll tests have been used to determine build-up and limit cycle characteristics of wing rock. Flow visualization techniques were also utilized in order to track vortex positions. The characteristics of the limit cycle (oscillation amplitude and frequency) were compared in detail with reference results obtained in other laboratories. An analytical nonlinear model was derived. Parameters were identified by means of the least-squares approximation of experimental data with coherent initial conditions. The consistency of time histories, reproduced by numerical integration, was also analyzed. This formulation correctly predicts stable limit cycles for a wide range of airspeeds, angles of attack and release roll angles.

Keywords: Aircraft dynamics, system modeling and identification, wind tunnel testing.

Nomenclature

a_i	=	nondimensional coefficients
b	=	wing span
c	=	wing root chord
C_l	=	rolling moment coefficient (L/qSb)
f	=	oscillation frequency
I_{xx}	=	model inertia
k	=	reduced oscillation frequency ($\pi f b/V$)
L	=	rolling moment
q	=	dynamic pressure ($\rho V^2/2$)
S	=	model wing surface
S_{wt}	=	wind tunnel cross-section
Re	=	Reynolds number (based on c)
t	=	time
$\hat{t}$	=	nondimensional time (t/t^*)
t^*	=	reference time ($b/2V$)
TPI	=	Politecnico di Torino
V	=	airspeed

Greek symbols

α	=	angle of attack
β	=	angle of sideslip
φ	=	roll angle
φ_0	=	release roll angle
$\Delta\varphi$	=	oscillation amplitude in roll
ρ	=	air density
$\dot{}$	=	time derivative

1. Introduction

Wing rock is an oscillatory rolling motion of an aircraft with increasing amplitude up to a limit cycle. The final state is generally stable and characterized by both large roll attitudes and coupling with directional modes. Handling qualities are obviously compromised and the maneuvering capabilities degrade in terms of the maximum achievable angle of attack. Moreover the presence of wing rock in the approach or landing phase can have very serious consequences on the operational safety of the aircraft.

This phenomenon, arising from a nonlinear aerodynamic mechanism [1], has been documented in flight at a high angle of attack, on configurations with slender forebodies and highly swept wing planforms combined with leading edge extensions. High speed civil transport and combat aircraft can fly under conditions where this self-induced oscillatory rolling motion is observed.

The aerodynamic regime on these configurations is dominated by vortical flows [2]. Evidence is given that, during wing rock oscillations, the normal position in the cross-flow plane of vortex cores is affected by hysteresis. The roll angular velocity greatly influences both the pressure distribution on the wing surface and the roll damping. Furthermore, the vortex strength varies during the wing rock process. Free-to-roll and forced oscillation tests on slender delta wings indicated that wing rock build-up is substantially promoted by roll damping decrease at high angles of attack.

The systematic approach to the study of wing rock is based on wind-tunnel experimental investigations of roll dynamics for highly swept delta wing models [3–9]. These simplified geometries exhibit stable limit cycles and correctly reproduce the dominant effect of primary wing vortices. Differently, the analysis of complete aircraft roll dynamics is quite difficult, as the relevant aerodynamic interactions between forebody, lifting surfaces, and empennages may alter the onset mechanism of wing rock.

Diverse mathematical formulations of the differential equation governing the single-degree-of-freedom approximation of the roll mode were suggested and validated by means of a complete parametric identification using both numerical simulations and experimental data:

$$C_l(t) = a_0 + a_1\varphi + a_2\dot{\varphi} + a_3|\varphi|\dot{\varphi} + a_4|\dot{\varphi}|\dot{\varphi} \qquad \text{(Ref. [1])},$$

$$C_l(t) = a_0(\varphi) + a_1(\varphi)\dot{\varphi} + a_2(\varphi)\dot{\varphi}^2 + a_3(\varphi)\dot{\varphi}^3 + a_4(\varphi)\dot{\varphi}^4 \qquad \text{(Ref. [8])},$$

$$C_l(t) = a_1\varphi + a_2\dot{\varphi} + a_3\varphi^3 + a_4\varphi^2\dot{\varphi} + a_5\varphi\dot{\varphi}^2 \qquad \text{(Ref. [10])}.$$

Accurate modeling of wing rock is essential in order to design control systems able to suppress or alleviate this form of degraded stability. As a matter of fact, one problem with these analytical studies is that the mathematical model cannot be directly related with the understanding of the flowfield characteristics.

2. Experimental Activity

Free-to-roll experiments were performed on a delta wing for $\alpha = 21$–$45°$, $V = 15$–40 m/s, $\mathrm{Re} = 486000$–1290000 and $\varphi_0 = 0$–$90°$.

The experimental tests were carried out in the D3M low speed wind tunnel at Politecnico di Torino. The test section is circular (3 m in diameter). The turbulence level is 0.3% at $V = 50$ m/s.

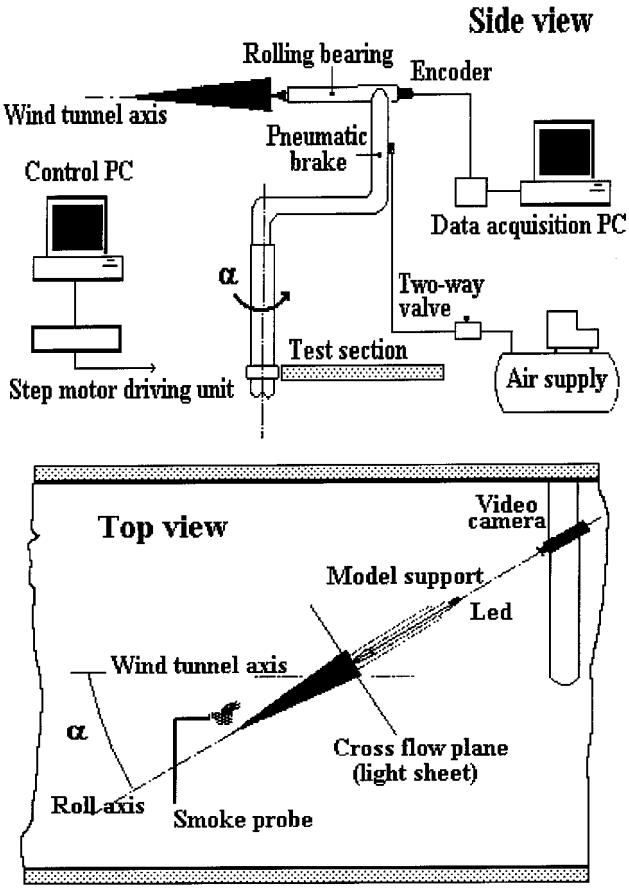

Figure 1. The experimental setup.

The model was a 80° delta wing with sharp leading and trailing edges, made in aluminum alloy. The dimensions are: root chord $c = 479$ mm, span $b = 169$ mm, thickness 12 mm, bevel angle 20°. The wing longitudinal body axis and the bearings axis coincide. The rotating system was statically balanced.

The C-shaped support (Figure 1) was mounted on a vertical strut which was able to rotate so that the angle of attack could change while the model centroid remained at the center of the test section.

The model was connected to a horizontal shaft supported by rolling bearings. In order to minimize the friction of the angular transducer, the motion of the wing was measured by an optical encoder, linked with the rotating shaft using an elastic joint without backlash. This digital transducer was able to provide a resolution of 0.45°/bit.

A pneumatic brake was adopted to keep the wing in the initial angular position. During wind-on runs, a trigger signal was sent by the operator to the data acquisition unit and the model was released by a pneumatic cylinder fitted inside of the vertical arm of the C-shaped support.

The digital signals generated by the encoder, which identify the sign, the increment and the zero crossing of $\varphi(t)$, were conditioned by an electronic device consisting of an incremental counter and a 12 bit digital to analog converter. Both the analog output and the zero crossing

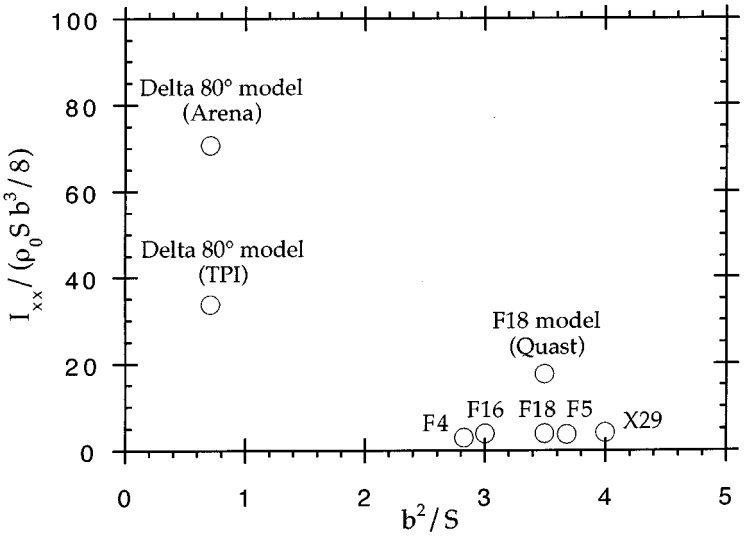

Figure 2. Aspect ratio and nondimensional rotational inertia for different models and aircraft.

trigger signal were multiplexed with a rate of 50 samples/s over a period of 45 s. The data acquisition system was based on a 12 bit analog to digital converter and an oscilloscope for the real time signal monitoring.

The amplitude and the oscillation frequency of the limit cycles were identified after the numerical elaboration of the time histories $\varphi(t)$ with a spectral analyzer. The angular rates were evaluated numerically.

The rolling moment coefficient was evaluated considering that

$$C_l = \frac{I_{xx}}{qSb}\ddot{\varphi}, \tag{1}$$

where $I_{xx} = 1.0117 \times 10^{-3}$ kg m^2 is the moment of inertia about the roll axis. The coefficient C_l includes the effect of friction (C_{l_f}):

$$C_l = C_{l_{\text{aer}}} + C_{l_f} = C_{l_{\text{aer}}} + C_{l_{\text{of}}} + \mu_f \dot{\varphi}, \tag{2}$$

where $C_{l_{\text{aer}}}$ is the aerodynamic rolling moment coefficient. The nonlinear term μ_f was neglected taking into account that the limit cycle parameters $(\Delta\varphi, k)$ measured at TPI for Re $=$ 636000 are very similar to those presented in [5] for comparable test conditions (see Figure 3). The experimental setup adopted by Arena and Nelson is definitely frictionless as the rotating shaft is supported by air bearings. Furthermore, the tests performed by Hanff in [11] on a free-to-roll apparatus similar to the TPI rig demonstrate that only the constant friction term $C_{l_{\text{of}}}$ is required to model the system friction, regardless of the angular velocity and loads acting on the wing. A direct measurement of the static torque due to friction in wind-off conditions confirmed that the term $C_{l_{\text{of}}}$ is very small ($L_{\text{of}} = 4.5 \times 10^{-4}$ Nm) for the TPI oscillatory rig. It must also be observed that the wing oscillations were always immediately triggered as the pneumatic brake fitted to the TPI support system was released, even for $\varphi_0 \approx 0$ (see Figure 6).

A complete analysis of the effects of model axis of rotation and friction due to bearings on wing rock experimental data is also given in [12].

An extensive derivation of criteria for inertia similitude between different models, or model and aircraft, is given in [13, 14]. These criteria state that similitude is ensured when the two

Table 1. The geometrical characteristics of several 80° delta wing models.

Model	c [mm]	b [mm]	S/S_{wt}
Ref. [4]	1760	620	0.041
Ref. [3]	428	150	0.032
Ref. [5]	422	149	0.085
Ref. [8]	200	70	0.019
Ref. [9]	479	169	0.006

configurations possess the same nondimensional ratio $I_{xx}/\rho b^5$. Hence, the nondimensional inertias for different models and aircraft are compared in Figure 2. This analysis demonstrates that relevant scaling factors are required in order to compare in-flight wing rock with free-to-roll experiments. Similar factors apply for models with the same geometry tested in different wind tunnels.

The comparison of different reference model geometries and blockage factors S/S_{wt} is presented in Table 1.

The results presented (Figure 3) are substantially similar to those given in [5] by Arena and Nelson. The agreement with Nguyen et al. [4] is limited to the lower angle of attack range ($\alpha \leq 35°$). Important differences are found among the majority of the experimental data and the oscillation amplitudes measured in [3] by Levin and Katz. The maximum is shifted ($\Delta\alpha = -7°$) and the amplitude is reduced. The explanation of these discrepancies is the peculiar model geometry which altered the vortex dynamics, due to the presence of a fuselage. As a matter of fact, even the onset of vortex breakdown was consistently anticipated ($\Delta\alpha = -10°$).

The comparisons performed for the oscillation frequency (Figure 3) confirm the accordance with the measurements presented in [5]. The trend of $k(\alpha)_{\text{TPI}}$ is coincidental but shifted to higher values. This difference is a direct consequence of the different rotational inertia of the experimental apparatus adopted in [5]. The experiments performed by Arena and Nelson establish that the oscillation frequency is proportional to $1/\sqrt{I_{xx}}$ and that the amplitude $\Delta\varphi$ is not substantially changed by I_{xx}. Anyway, the inertial scaling of the results performs correctly, as confirmed by the comparison presented in Figure 3.

The onset of stable wing rock oscillations α_{ON} depends on airspeed. Some tests were performed reducing the angle of incidence during the oscillation of the model, in order to evaluate the lower limit α_{OFF} for the stability of the limit cycle (Table 2).

A set of experiments was devoted to the analysis of the limit cycle characteristics after different initial conditions φ_0. The conclusion is that both amplitude and frequency are not significantly influenced by this parameter (Figure 4), although different build-up time histories are established by increasing the release roll angle. Roll divergence after the model release was never observed for $-90° < \varphi_0 < +90°$.

Some visualizations were also performed at $V = 10$ m/s with the aim of tracking the vortex dynamics in the cross-flow plane. A smoke probe was positioned in front of the model apex (Figure 1). A sheet of light was placed along the trailing edge (section at $x/c = 1.0$) and a video camera was aligned with the rotation axis that was marked by a led. The images

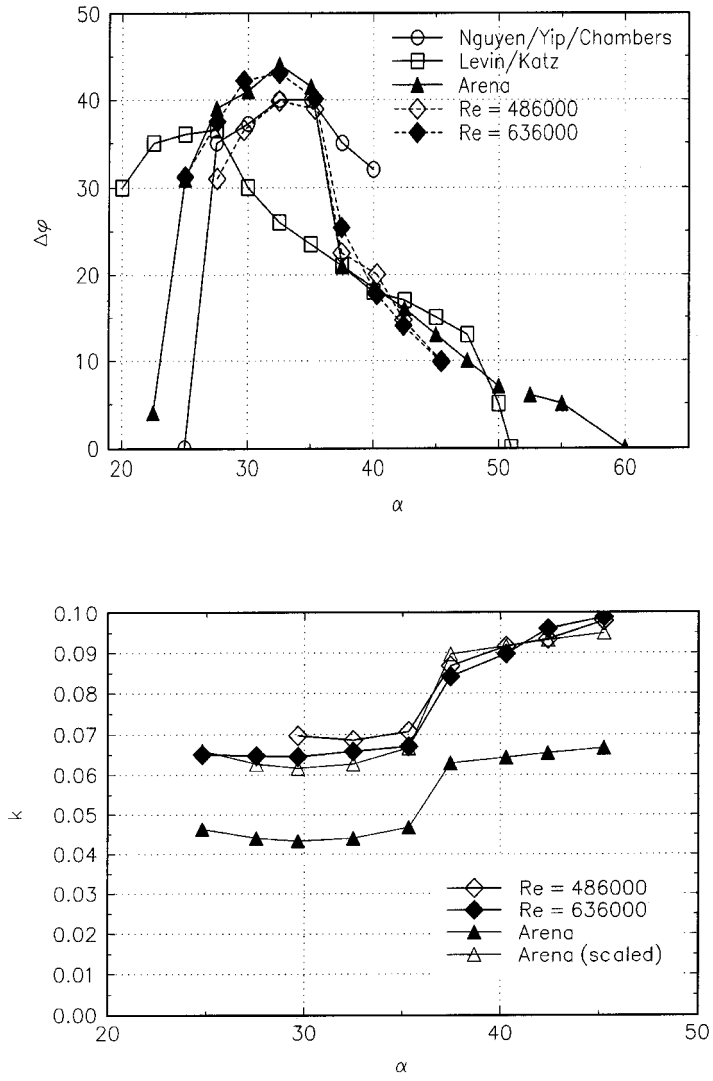

Figure 3. The experimental data at different angles of attack.

Table 2. The lower stability boundaries of wing rock limit cycle.

Re	α_{ON} [deg]	α_{OFF} [deg]
486000	27	25
636000	25	23
959000	25	21
1290000	25	21

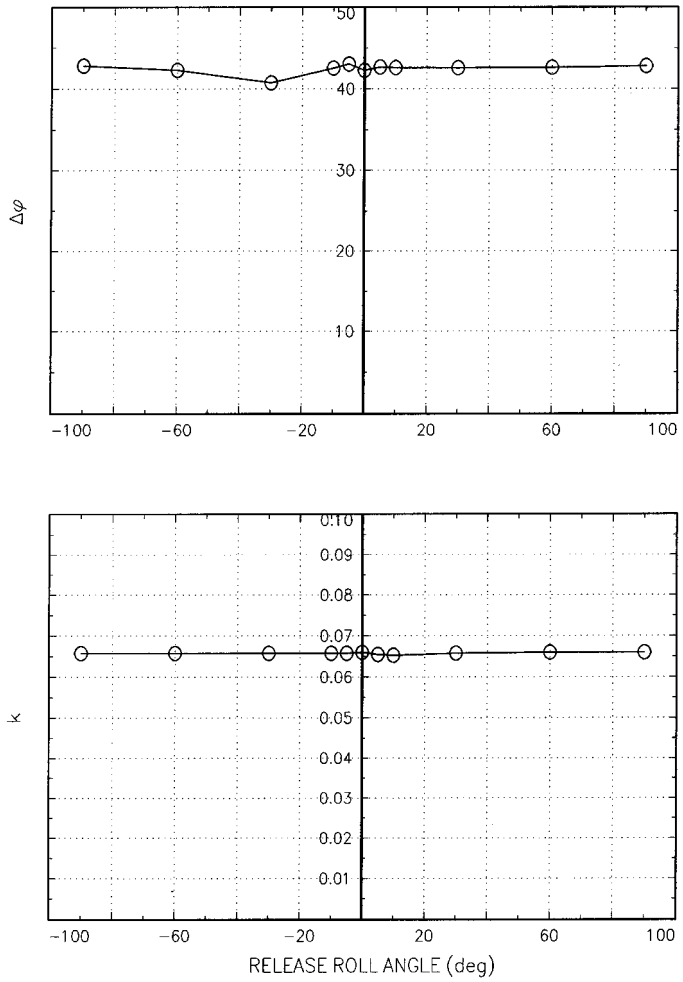

Figure 4. The effect of release roll angle φ_0 on limit cycle oscillation amplitude and frequency ($\alpha = 32.5°$, Re = 636000).

were digitized step by step so that the dynamic vortex core displacements could be accurately measured and reduced to the body axes frame.

The tracking of the primary vortex positions in the cross-flow plane supports the validity of some experimental observations [5] concerning the explanation of the driving mechanism of wing rock.

The hysteresis of the normal coordinate z/b is dominant (Figure 5), while only a marginal time lag is shown for the spanwise vortex core position y/b. During the limit cycle, the vortex cores move symmetrically on the two parts of the wing so that $z_r(\hat{t}) = z_l(\hat{t} \pm \pi/k)$.

The reduction of the distance z/b between the vortex core and wing upper surface generates a local increment of suction. The opposite occurs when the normal distance is increased. Therefore, the term $(z_r - z_l)$ becomes an indicator of the differential lift acting on the two semi-wings of the rolling model. The cyclic variation of the asymmetry parameter $(z_r - z_l)$ proves that both the dynamic displacement of the two primary vortices and the restoring aerodynamic moment are coupled.

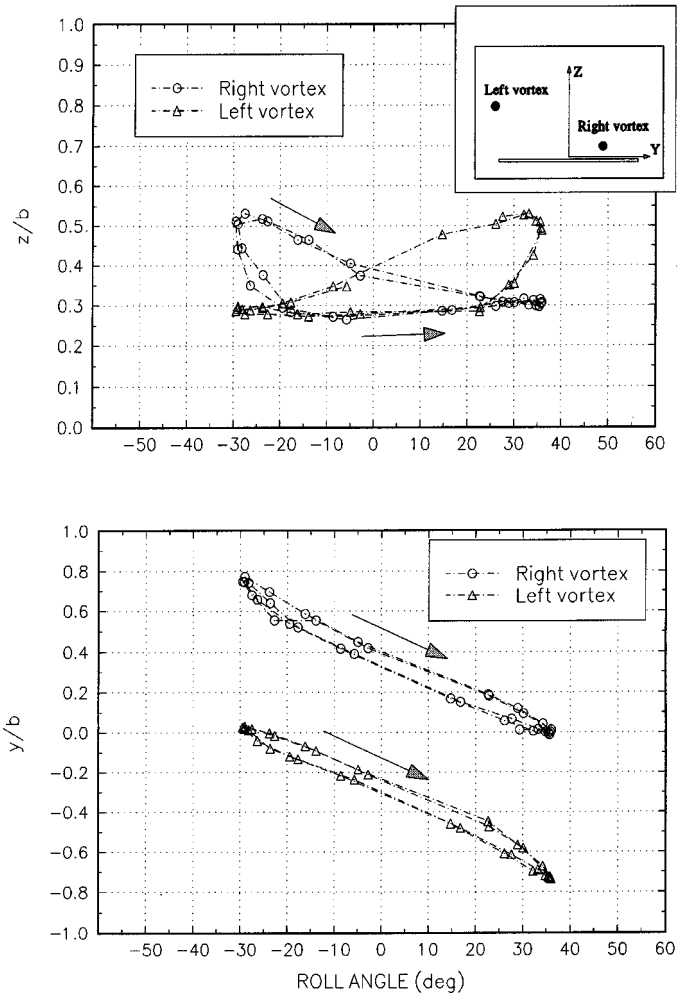

Figure 5. The vortex core displacement in dynamic conditions ($\alpha = 32.5°$).

The limit cycle presented in Figure 5 is not affected by vortex breakdown. Hence, no direct relationship can be established between the onset of wing rock and the stability of the primary vortices. On the contrary, the amplitude and the frequency of the limit state are strongly coupled with this phenomenon which was observed for $\alpha > 37°$. The sudden changes of the parameters $\Delta\varphi$ and k for $35° < \alpha < 37°$ are important consequences of vortex burst which modifies the dynamic stability of the rolling system [5].

Furthermore, the variability of the oscillation amplitude $\sigma_{\%}$ is larger for $\alpha > 37°$ due to the natural unsteadiness of vortex breakdown locations ($\sigma_{\%} = 6\%$ at $\alpha = 32°$ and $\sigma_{\%} = 20\%$ at $\alpha = 37°$).

3. Mathematical Modeling

The phase plane representation of the wing rock oscillations (Figure 6) shows that the phenomenon is dominated by nonlinear damping and a relationship can be established with the

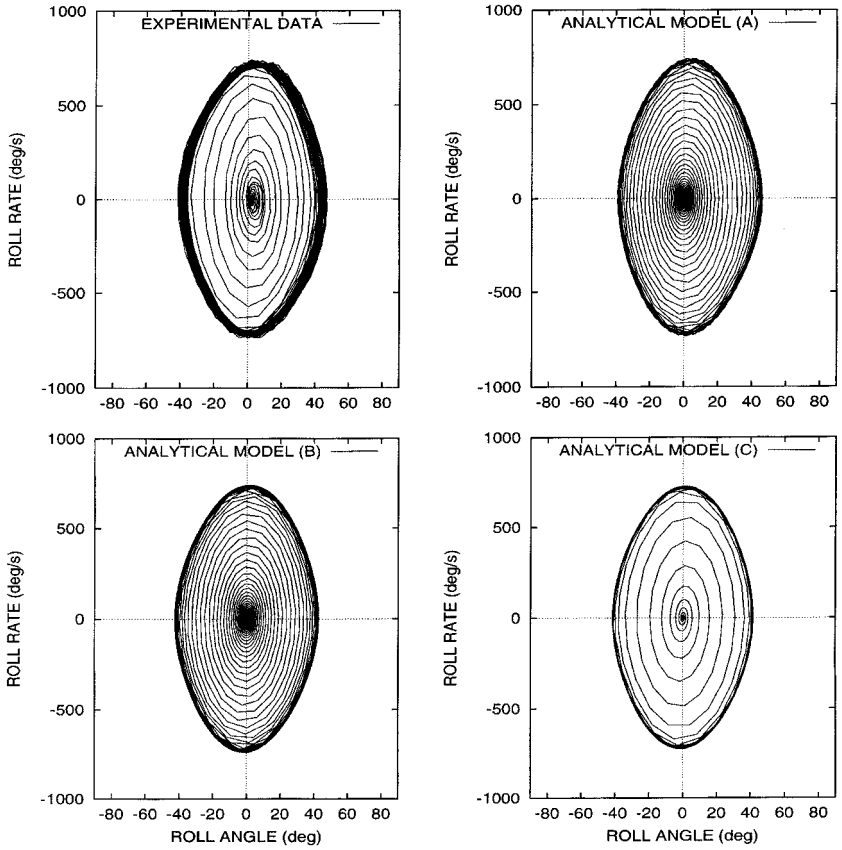

Figure 6. Comparison of experimental data ($\alpha = 32.5°$, Re $= 636000$, $\varphi_0 \approx 0$) and different analytical models (Model **A**: $\ddot{\varphi} + a_0\varphi + a_1\dot{\varphi} + a_2\dot{\varphi}^2 + a_3\varphi^3 + a_4\varphi^2\dot{\varphi} = 0$; Model **B**: $\ddot{\varphi} + a_0\varphi + a_1\dot{\varphi} + a_2\varphi\dot{\varphi}^2 + a_3\varphi^3 + a_4\varphi^2\dot{\varphi} = 0$; Model **C**: $\ddot{\varphi} + a_0\varphi + a_1\dot{\varphi} + a_2|\dot{\varphi}|\dot{\varphi} + a_3\varphi^3 + a_4\varphi^2\dot{\varphi} = 0$).

analytical models of some single-degree-of-freedom limit cycle oscillators (Duffing's and Van der Pol's equations).

The shape of the orbits is elliptic, reflecting the existence of a family of almost sinusoidal solutions:

$$\varphi(t) = a(t)\cos(\omega_n t + b(t)), \tag{3}$$

where $a(t)$ is the amplitude and $b(t)$ is the phase.

Anyway, during the initial cycles of motion, the trajectories with larger amplitudes deform from the purely elliptical shape. This behavior is often seen in dynamical systems which contain a nonlinear restoring moment.

The experimental analysis of the roll attractor [9] demonstrates that the limit cycle is not dependent on the initial condition φ_0 and the same stable orbits are found with both internal and external release roll angles.

Different analytical nonlinear models were considered in [9] and the following best fit formulation was identified:

$$\ddot{\varphi} + a_0\varphi + a_1\dot{\varphi} + a_2|\dot{\varphi}|\dot{\varphi} + a_3\varphi^3 + a_4\varphi^2\dot{\varphi} = 0, \tag{4}$$

where the time derivatives are nondimensional.

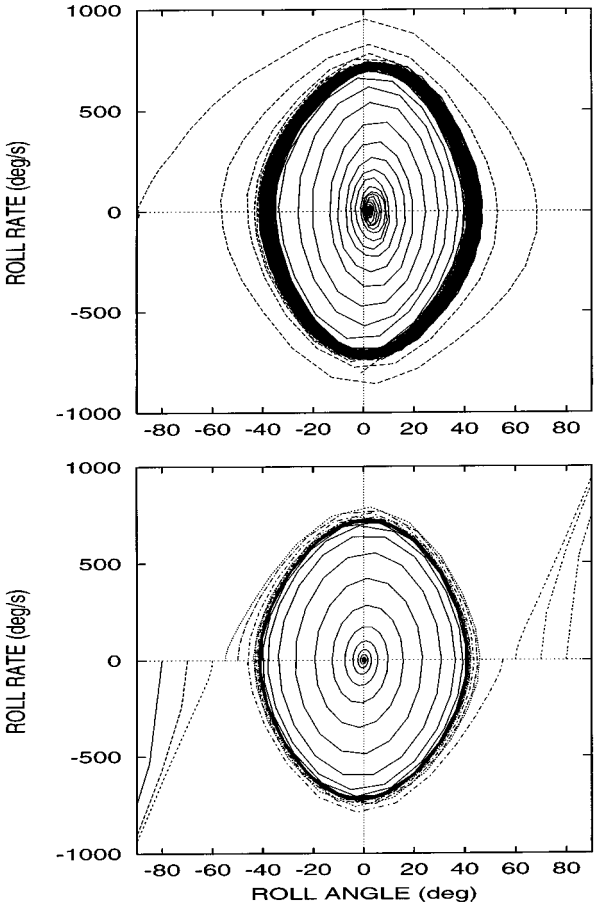

Figure 7. The phase plane plot for different initial conditions: comparison of experimental (top) and analytical (bottom) results ($\alpha = 32.5°$).

The effect of the term $a_2|\dot{\varphi}|\dot{\varphi}$ on model accuracy is presented in Figure 6 where different implementations are compared. Although the use of absolute values may introduce some complexity in the analysis [10], it is actually required for a correct reproduction of the build-up phase.

The effect of initial conditions on model time domain response is given in Figure 7. The mathematical model predicts roll divergence for initial release roll angles $\varphi_0 > 60°$ that is not consistent with the available experimental results obtained at TPI. This discrepancy can be related with the divergence of the restoring moment due to the softening term $a_3\varphi^3$ that underestimates the wing dihedral stability for larger roll displacements. Anyway, limit cycle characteristics and build-up dynamics are accurately predicted for realistic release roll angles $\varphi_0 < 60^o$.

The parameters a_i (Figures 8–12) were identified by means of least-squares approximation of the experimental results. The influence of airspeed on these coefficients is evident for a_1, a_2 and a_4 in the α region where vortex burst occurs. As a matter of fact, the combined effect of roll rate and airspeed (i.e. the increase/decrease of $\hat{p} = \dot{\varphi}b/2V$) alters the damping generated by the presence of vortex breakdown. The consequence is that limit cycle characteristics are

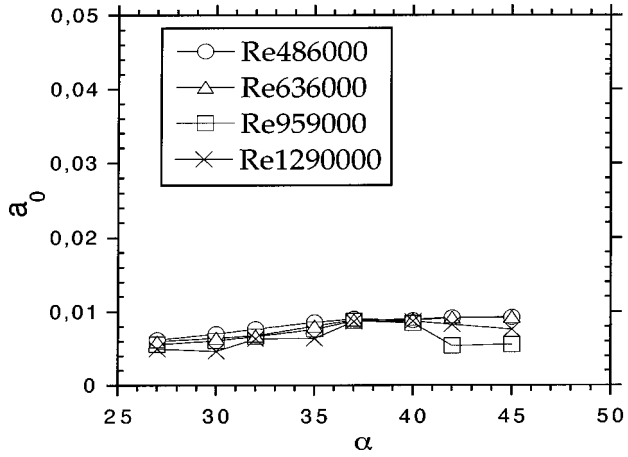

Figure 8. The coefficient a_0 in the analytical model.

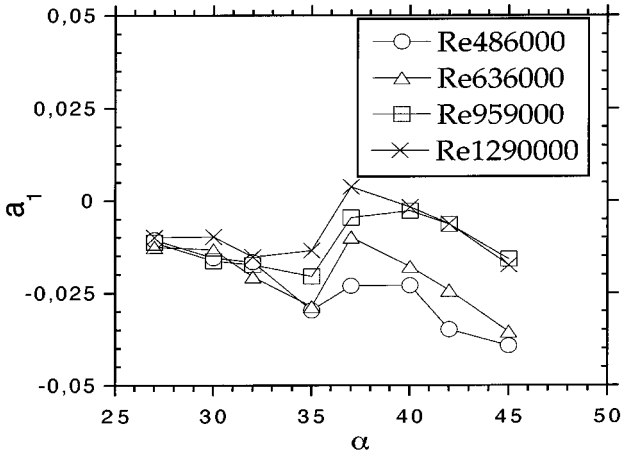

Figure 9. The coefficient a_1 in the analytical model.

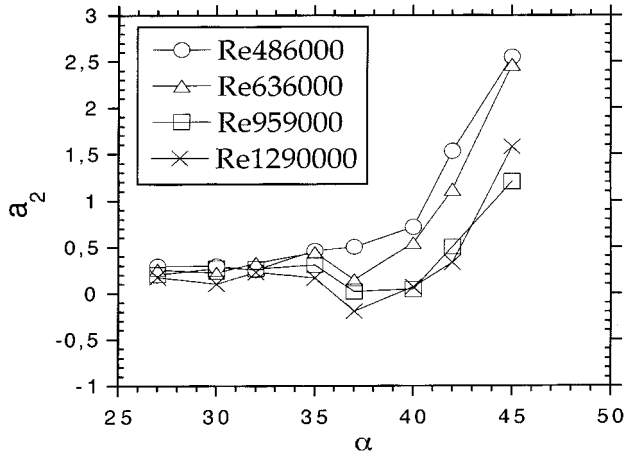

Figure 10. The coefficient a_2 in the analytical model.

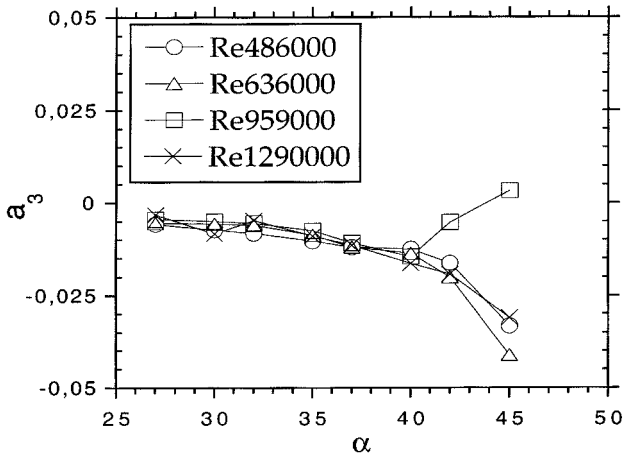

Figure 11. The coefficient a_3 in the analytical model.

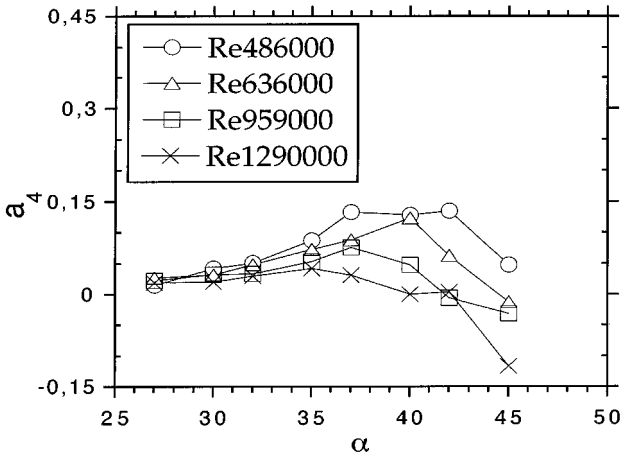

Figure 12. The coefficient a_4 in the analytical model.

fairly constant with airspeed while build-up dynamics (transient phase) is modified by this damping increase.

Differently, stiffness terms a_0 and a_3 are moderately affected by V (i.e. wing rock natural reduced frequency is substantially unchanged by the increase of airspeed), although a particular divergence from other data is observed for a_3 at high angle of attack at $V = 30$ m/s (Figure 11). This result is related to vortex breakdown unsteadiness, typically observed for this wing in the α range over 37°. Anyway, the minimal changes of the stiffness coefficients produce moderate increments of limit cycle amplitude $\Delta\varphi$ with airspeed [9].

4. Model Analysis

The restoring moment $a_0\varphi + a_3\varphi^3$ (Figure 13) exhibits a typical trend with a softening of linear stiffness a_0. As a consequence, the system is statically divergent for $\varphi > \sqrt{-a_0/a_3}$. The reduced order model

$$\ddot{\varphi} + a_0\varphi + a_3\varphi^3 = 0 \tag{5}$$

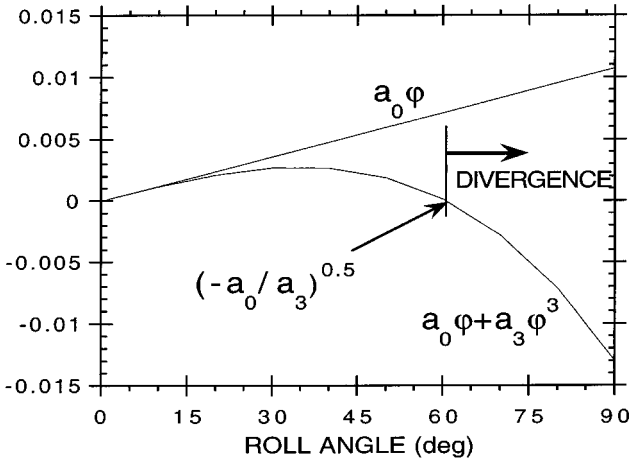

Figure 13. The effect of roll angle on restoring moment in the analytical model ($\alpha = 32.5°$).

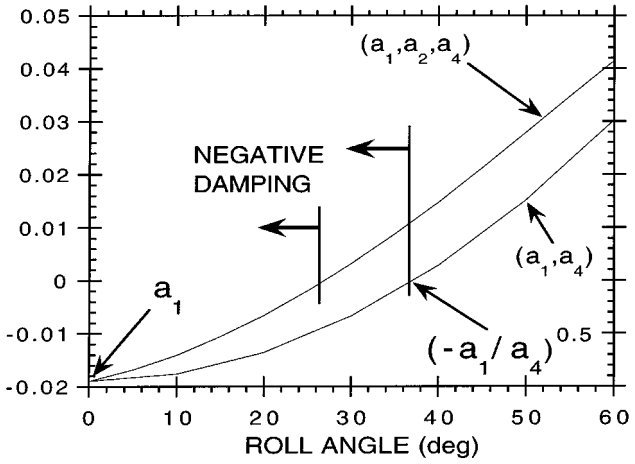

Figure 14. The nonlinear effect of roll angle on damping term in the analytical model ($\alpha = 32.5°$).

describes an undamped system with nonlinear stiffness.

Assuming that $\varphi(\hat{t}) = \Delta\varphi \sin k\hat{t}$, the locus of solutions (Figure 15) is given by the values $(\Delta\varphi, k)$ that respect the equation

$$1 - \frac{k^2}{a_0} + \frac{3}{4} \cdot \frac{a_3}{a_0} \Delta\varphi^2 = 0. \tag{6}$$

The damping coefficient $(a_1 + a_4\varphi^2)$ is nonlinear and negative for $\varphi < \sqrt{-a_1/a_4}$ (Figure 14). The system is dynamically unstable for lower roll angles becoming stable as φ increases up to the inversion point. The coordinate for this dynamic stability cross-over is not coincident with limit cycle amplitude, as the stability of final state occurs when

$$E = qSb \oint_{\ell} C_l(\varphi)\, \mathrm{d}\varphi = 0. \tag{7}$$

This condition is required for the balance between dissipation and generation of energy and for a stable oscillatory limit cycle.

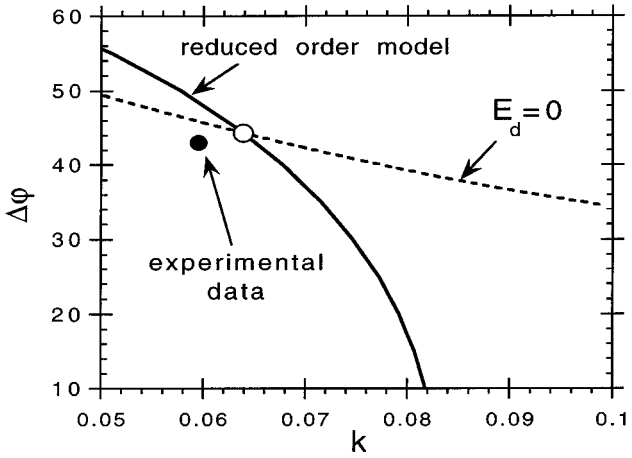

Figure 15. Comparison of experimental results with a reduced order analytical model ($\alpha = 32.5°$).

Dynamic stability and limit cycle characteristics are also influenced by the additional damping produced by the term $a_2|\dot{\varphi}|\dot{\varphi}$. An equivalent linear damping can be derived [15] if the limit cycle is represented by the function $\varphi(\hat{t}) = \Delta\varphi \sin k\hat{t}$. The equivalence is established assuming that the dissipation of energy over a complete cycle is the same ($T = 2\pi/k$):

$$
\begin{aligned}
E_d &= 4\int_0^{T/4} a_n|\dot{\varphi}|^n \,\mathrm{d}\varphi \\
&= 4\int_0^{T/4} a_n|\dot{\varphi}|^{n+1} \,\mathrm{d}\hat{t} \\
&= 4a_n k^n \Delta\varphi^{n+1} \int_0^{\pi/2} |\cos k\hat{t}|^{n+1} \,\mathrm{d}k\hat{t} \\
&= \pi a_n k^n \Delta\varphi^{n+1} \gamma_n,
\end{aligned}
$$

where

$$
\gamma_n = \frac{4}{\pi}\int_0^{\pi/2} |\cos k\hat{t}|^{n+1} \,\mathrm{d}k\hat{t}. \tag{8}
$$

Hence, the equivalent linear damping term a_{eq} is obtained as

$$
a_{\mathrm{eq}} = a_2 k \Delta\varphi \frac{\gamma_2}{\gamma_1} = a_2 k \Delta\varphi \frac{8}{3\pi}. \tag{9}
$$

This last equation allows one to include the damping coefficient $a_{eq} \approx a_2|\dot{\varphi}|$ in the nonlinear model (Figure 14). As a consequence, the cross-over point is shifted to lower roll angles with a stabilizing effect.

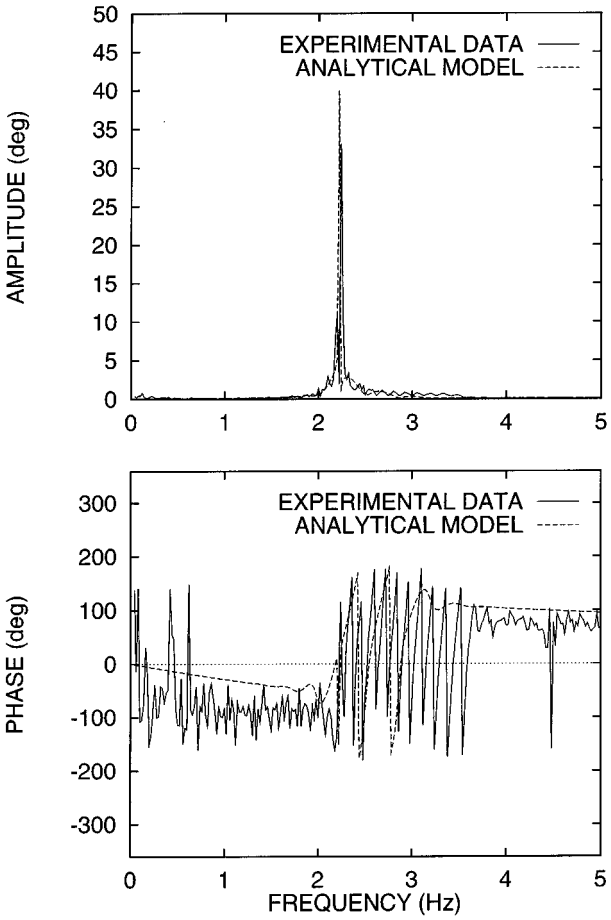

Figure 16. Comparison of experimental and analytical spectral data ($\alpha = 32.5°$, Re = 636000).

The locus of solutions $(\Delta\varphi, k)$ that respect

$$E_d = \oint_{\ell} (a_1 + a_2|\dot{\varphi}| + a_4\varphi^2)\dot{\varphi}\, d\varphi = 0 \tag{10}$$

is also compared in Figure 15 with the solutions for the undamped system. The stable limit cycle is quite accurately estimated by the intersection of the two plots for Equations 6 and 10. Overprediction of frequency and amplitude is related with the approximation introduced in the reduced order system (decoupling of restoring and damping moments).

5. Model Validation

Time domain validations were performed by comparing numerical integrations of the mathematical model with experimental data (Figure 6).

The prediction of the wing rock oscillations is always accurate for $\varphi_0 < \Delta\varphi$. On the contrary an unexpected divergence is found for external initial conditions ($\varphi_0 > 60°$) modeled numerically by Nayfeh et al. [10].

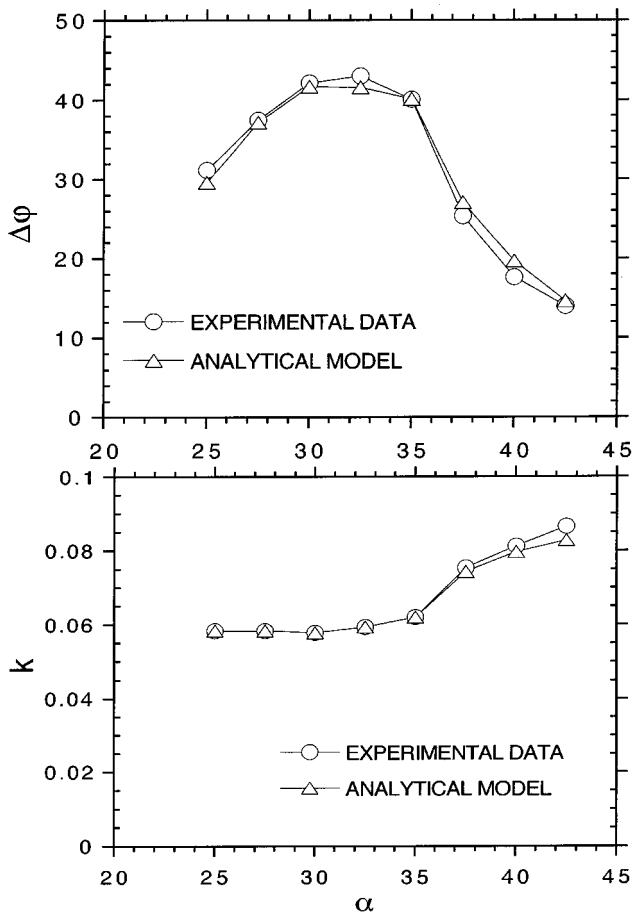

Figure 17. Comparison of experimental and analytical limit cycle characteristics (Re = 636000).

The discrepancy between experiments and analytical approximations is explained considering that the model includes a cubic softening term. Previous studies [10] proved that the importance of this contribution is related to the divergence of the motion starting with peculiar initial conditions, such as large φ_0. Hence, a correct mathematical model should include a cubic parameter $a_3(\alpha, \varphi_0)$ evaluated from experimental data with different release roll angles. This model improvement has no practical impact taking into account that the onset of in-flight wing rock is triggered for moderate aircraft initial roll angles φ_0.

Frequency domain validation (Figure 16) also confirms the accurate reproduction of the spectral components of time histories $\varphi(t)$ during the stable oscillatory phase. Differently, an approximate reconstruction of build-up frequencies is obtained by the analytical model that smoothes the frequency stretching clearly observed in the very initial phase of the experimental measurements (clustering of roll trajectories in Figure 6).

Complete numerical simulations show that overall limit cycle characteristics are correctly reproduced by the analytical model (Figure 17).

6. Concluding Remarks

Free-to-roll experiments were performed on a 80° delta wing undergoing self-induced wing rock oscillations. The tests were carried out at different angles of attack, airspeeds and initial roll angles in order to investigate the influence of the experimental parameters on the limit cycle.

The amplitude of the oscillatory mode is a nonlinear function of incidence and its maximum is reached at $\alpha = 32.5°$. Stable limit cycles were observed for $\alpha \geq 25°$.

Comparison with other reference experimental data confirms that the measurements performed at TPI are accurate.

The hysteresis of vortex core position along the Z axis, which is the primary explanation of the driving mechanism of wing rock, was evaluated by means of flow visualizations.

Vortex breakdown and the onset of wing rock are not related by a direct mechanism for this wing. The experimental results confirm that the vortex breakdown alters the limit-cycle characteristics with a reduction of $\Delta\varphi$ while the nondimensional oscillation frequency k increases abruptly.

The limit cycles are stable for $0 < |\varphi_0| < 90°$ and $\dot{\varphi}_0 = 0$. The amplitude and the frequency of the final state are not influenced by φ_0.

The oscillatory behavior was reproduced by an analytical model, based on a parametric analysis of the experimental results. The model was validated (time domain and frequency domain validation). The contributions of coefficients of the nonlinear terms in the mathematical model were also discussed.

References

1. Hsu, C. H. and Lan, C. E., 'Theory of wing rock', *Journal of Aircraft* **22**(10), 1985, 920–924.
2. Katz, J., 'Wing-vortex interactions and wing rock', *Progress in Aerospace Sciences* **35**, 1999, 727–750.
3. Levin, D. and Katz, J., 'Dynamic load measurements with delta wings undergoing self induced roll oscillations', *Journal of Aircraft* **21**(1), 1984, 30–36.
4. Nguyen, L. T., Yip, L. P., and Chambers, J. R., 'Self induced wing rock of slender delta wings', in *Proceedings of the AIAA Atmospheric Flight Mechanics Conference*, Albuquerque, NM, AIAA, Washington, DC, 1981.
5. Arena, Jr., A. S., 'An experimental and computational investigation of slender wings undergoing wing rock', Ph.D. Dissertation, University of Notre Dame, Indiana, 1992.
6. Arena, Jr., A. S. and Nelson, R. C., 'An experimental study of the nonlinear dynamic phenomenon known as wing rock', AIAA Paper 90-2812, 1990.
7. Arena, Jr., A. S. and Nelson, R. C., 'Measurement of unsteady surface pressure on a slender wing undergoing a self induced oscillation', *Experiments in Fluids* **16**(6), 1994, 414–416.
8. Yoshinaga, T., Tate, A., and Noda, J., 'Wing rock of delta wings with an analysis by the phase plane method', in *Proceedings of the AIAA Atmospheric Flight Mechanics Conference*, Monterey, AIAA Washington, DC, 1993.
9. Guglieri, G. and Quagliotti, F. B., 'Experimental observation and discussion of the wing rock phenomenon', *Aerospace Science and Technology* **1**(2), 1997, 111–123.
10. Nayfeh, A. H., Elzebda, J. M., and Mook, D. T., 'Analytical study of the subsonic wing rock phenomenon for slender delta wings', *Journal of Aircraft* **26**(9), 1989, 805–809.
11. Hanff, E. S., 'Large amplitude oscillations', AGARD-R-776, 1991.
12. Kostandinopoulos, P., Mook, D. T., and Nayfeh, A. H., 'Subsonic wing rock of slender delta wings', *Journal of Aircraft* **22**(3), 1985, 223–228.
13. Quast, T., Nelson, R. C., and Fisher, D. F., 'A study of high alpha dynamics and flow visualization for a 2.5% model of the F-18 HARV undergoing wing rock', in *Proceedings of the AIAA Applied Aerodynamics Conference*, Baltimore, MD, 1991.

14. Quast, T., ‘A study of high alpha dynamics and flow visualization for a 2.5% model of the F-18 HARV undergoing wing rock’, MS Thesis, University of Notre Dame, IN, 1991.
15. Nocilla, S., *Meccanica Superiore per Ingegneri*, Levrotto & Bella, Torino, Italy, 1996.